Science in China Series D: Earth Sciences

Small-scale upper mantle convection and orogeny of Tianshan Mountains in China

LIU Jie†, LIU QiYuan, GUO Biao & SONG HuiZhen

State Key Laboratory of Earthquake Dynamics, Institute of Geology, China Earthquake Administration, Beijing 100029, China

In this study, from the travel time data recorded in the Tianshan passive seismic array experiment, we present the P-wave velocity structure of the upper mantle down to 660 km along the Kuqa-Kuitun profile in terms of seismic tomography technique. Based on the P-wave velocity model, we derive the corresponding 2D upper mantle density model. The 2D small-scale convection of the upper mantle underneath the Tianshan Mountains in China driven by the density anomalies is simulated using the hybrid finite element method combining with the marker-in-cell technique. The main features of the upper mantle convection and the reciprocation between the convection and mountain building are investigated. The results manifest that (1) in the upper mantle underneath the Junggar basin and North Tianshan exists a counterclockwise convection, which scale is ~ 500 km; (2) underneath the Tarim basin and South Tianshan exists a clockwise northward convection, which is relatively weak; (3) the convective velocity at the top of the upper mantle underneath the Tianshan Mountains in China should not be less than 20 mm/a, while considering the dependent of convective velocity on the viscosity; (4) the northward extrusion of the Tarim block plays a key role in the Cenozoic Tianshan mountain building and the present-day tectonic deformation of the Tianshan range is related closely to the upper mantle convection; and (5) the northward subduction of the Tarim block does not influence obviously the upper mantle convection.

Tianshan orogeny, mantle convection, orogeny, finite element method, marker-in-cell method

1 Introduction

In the present-day, the Tianshan range is the most active intracontinental mountain belt and it has been recognized as a natural laboratory for the intracontinental deformation and dynamics. Although many results concerning the geological structure and tectonic evolution of the mountains have been published, the most of them are limited merely to qualitative discussion and some basic problems about the Tianshan dynamics are still unclear [1].

It has been proved by the former studies that the rejuvenation of the Tianshan Mountains since Miocene is caused mainly by the collision between the Indian and Eurasia plates[2−5]. There are several proofs about the horizontal crustal compression in the mountain building, including the crustal shortening, the existence of the foreland basins on both sides of the Tianshan Mountains, as well as intensively active folding and thrust[6−9].

Based on the analysis of the P-wave travel time residuals, Vinnik and Saipbekova[10] proposed the mantle upwelling underneath the western Tianshan. They proposed that the uplift of the Tianshan Mountains could be related to the upper mantle convection. These ideas have been proved by the seismic tomographic study of Roecker et al.[11] and the receiver function analysis by Kosarev et al[12]. According to the analysis of the time delay of the PS conversions, Chen et al.[13] inferred that

Received November 13, 2006; accepted March 19, 2007
doi: 10.1007/s11430-007-0070-4
†Corresponding author (email: liujieigcea@gmail.com)
Supported by the National Natural Science Foundation of China (Grant No. 40234043)

there is a low-velocity zone in the upper mantle beneath the central Tianshan. This implies that there should be the thermal abnormalities in the upper mantle beneath the western Tianshan.

Based on the inversion of the gravity data, Fu et al.[14]w proposed the small-scale mantle convection beneath the Tianshan Mountains in China. Since the gravity data is merely an integrated result of densities of the earth's media, it will be necessary to verify the existence of the upper mantle convection. The influences of the mantle flow on the mountain building also need to be investigated.

In recent years, the results given by seismic tomography have been used widely in studies of the mantle convection [15, 16]. Former studies have demonstrated that the numerical simulation based on seismic tomographic data facilitates the quantitative study of the mantle deformation and movement.

From April of 2003 to September of 2004, the State Key Laboratory of Earthquake Dynamics, Institute of Geology, China Earthquake Administration (IGCEA), deployed a movable array consisting of 60 broadband seismic stations along the Kuqa-Kuitun profile across the Tianshan range[17]. According to the P-wave travel time data recorded by this array and regional network, Guo et al.[18] presented the tomographic images of the P-wave velocity structure of the crust and upper mantle down to 400 km along the Kuqa-Kuitun profile. In comparison with the former results, their results have a much higher resolution and provide a more convincible database for the numerical modeling of the mantle convection.

In this study, based on seismic tomographic results, we shall investigate the possibility and patterns of the small-scale mantle convection underneath the Tianshan Mountains in terms of the numerical modeling technique[19]. Our results manifest a counterclockwise convection driven by the density anomalies in the upper mantle underneath the Junggar basin and North Tianshan, whose scale reaches to about 500 km. The convective velocity on the top of the upper mantle underneath the Tianshan Mountains in China should not be less than 20 mm/a. Underneath the Tarim basin and South Tianshan exists also a clockwise northward convection, which is relatively weak. The northward extrusion of the Tarim block plays a key role in the Cenozoic Tianshan mountain building. However, it almost does not influence the upper mantle connection. These new results provide the evidence for investigating the Tianshan dynamics.

2 Method and data

In this study, we use the new method which combines finite element method (FEM) with the marker-in-cell (MIC) algorithm together. In this method, the Eulerian description is combined with the Lagrangian description in terms of the markers filling up in cell describing the material property. In terms of the marker configuration, the material movement in heterogeneous medium can be described. The method can refer to ref. [19].

Our numerical modeling is based mainly on the seismic tomography of the P-wave velocity structure of the crust and upper mantle[18]. Up to now, the result presented by ref. [18] is the most detailed tomographic image of the P-wave velocity structure of the upper mantle underneath the Tianshan Mountains in China.

Ref. [18], however, merely presents the P-wave velocity structure ranging over 0—400 km. Obviously, this is deficient for investigating the upper mantle convection. Thus, we reconstruct the P-wave velocity structure of the crust and upper mantle down to 660 km along the Kuqa-Kuitun profile by using the same method and the same database with those used in ref. [18]. In Figure 1 are shown the station map of the movable seismic array across the Tianshan Mountains and the regional network and the P-wave velocity perturbation of the crust and upper mantle along the Kuqa-Kuitun profile. Figure 1(b) manifests that the maximal perturbation of the P-wave velocity of the upper mantle along the profile reaches to ~6%. It can be inferred from this result that a significant density anomaly exists within the upper mantle underneath the Tianshan Mountains in China.

3 Model and boundary conditions

In principle, the mantle convection is a 3D problem. However, up to now, the resolution of all of the 3D seismic tomography in the Tianshan Mountains in China is larger than 160 km[20,21]. This is obviously too poor for the small-scale convection study. Therefore, our study will be limited to the 2D case. Usually, the lithosphere deformation in the orogenic belts takes place along the direction perpendicular to the mountain strike. We have the same case in the Tianshan range[6−9,22]. Since the array observational profile along Kuqa-Kuitun is almost perpendicular to the mountain strike, this

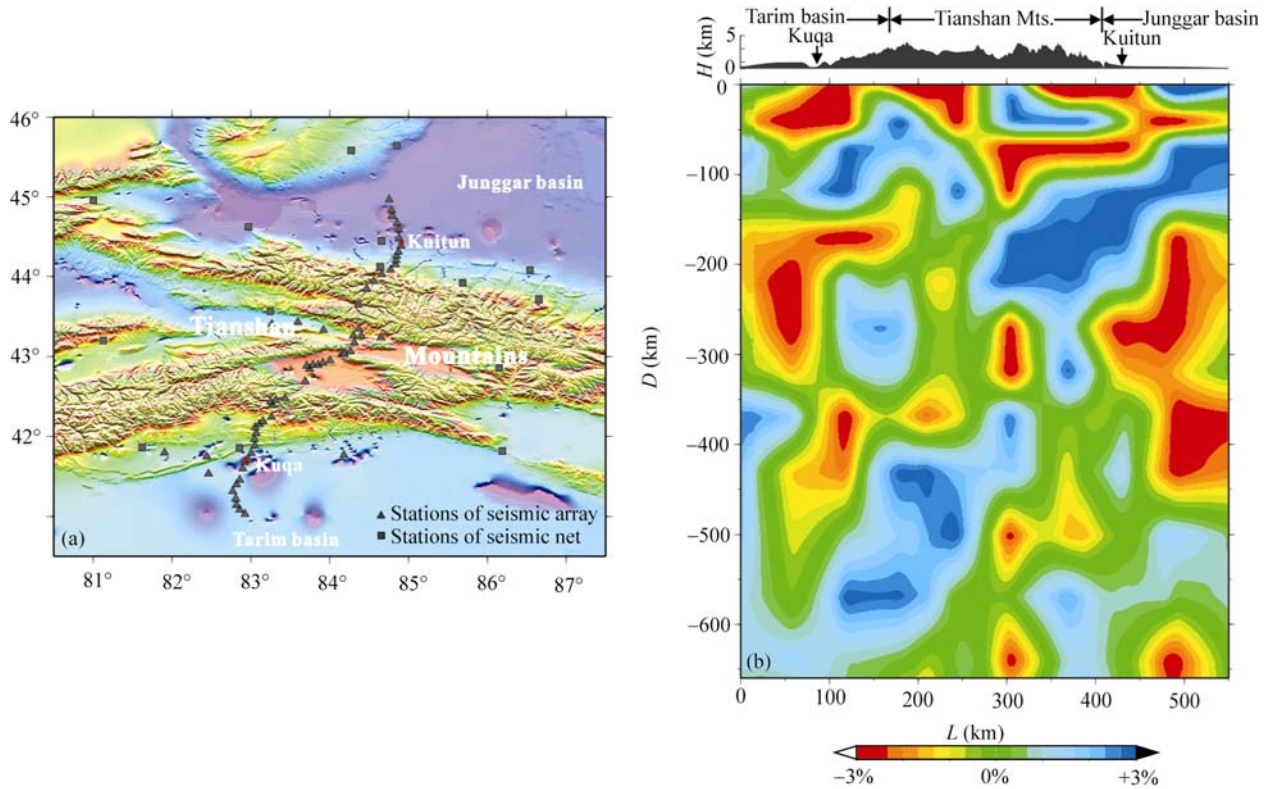

Figure 1 Distribution of seismic stations and P-wave perturbation structure. (a) Station map of the movable seismic array across the Tianshan Mountains and the regional network; (b) P-wave velocity perturbation of the crust and upper mantle along the Kuqa-Kuitun profile.

will be in favour of not only investigating the upper mantle deformation movement along the profile, but also understanding the influence of the upper mantle convection on the Tianshan orogeny.

3.1 Density model

Birch[23,24] presented at the earliest the regressive relation between the density and P-wave velocity for minerals. This is called the Birch's Law. Thus, based on the Birch's Law, the density model can be derived from the P-wave velocity structure of the crust and upper mantle.

The background level of the P-wave velocity perturbation shown in Figure 1 is based on the IASP91 model. The absolute P-wave velocity structure of the crust and upper mantle along the Kuqa-Kuitun profile can be recovered from the corresponding velocity perturbation. In fact, from the IASP91 model, we can have the linear relation between the density and P-wave velocity. Furthermore, we can have the density distribution of the crust and upper mantle along the Kuqa-Kuitun profile from the P-wave velocity structure and the density-velocity relation.

It should be pointed out that Figure 1(b) shows merely the P-wave velocity perturbation along the 550-km-long profile across the Tianshan Mountains. Thus, the corresponding density model derived from this velocity structure will be limited to the same range. To eliminate the influence caused by the boundary conditions, we have to extend further our density model toward both sides by horizontally elongating the density contours. Figure 2 shows the density model after the

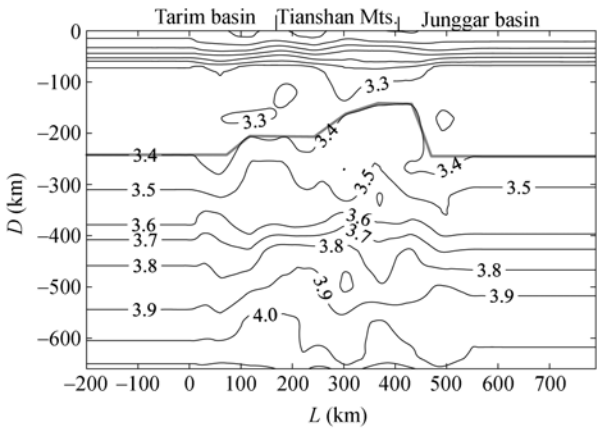

Figure 2 Density distribution of the crust and upper mantle along the Kuqa-Kuitun profile. The unit of the density is g/cm^3. The bold line denotes the lithosphere bottom boundary and the fine solid line denotes the density contour.

stretch, whose horizontal scale reaches to 990 km and the aspect ratio reaches to 1:1.5.

Figure 2 also shows the bottom boundary of the lithosphere corresponding to the density contour of 3.4 g/cm^3, which has been smoothed to remove the local undulation. The thickness of lithosphere shown in Figure 2 has a good agreement with the former researches[25,26].

3.2 Temperature and viscosity

The initial temperature field in our model is estimated from the normal temperature distribution in the crust and upper mantle[25,27]. In particular, we assume the temperature at the ground surface, the lithosphere bottom and the bottom of the upper mantle are 0℃, 1200℃ and 1700℃, respectively.

It is uneasy to estimate accurately the viscosity of the earth's medium. In general, the viscosity of the upper mantle should be in the range of $10^{19}-10^{21}$ Pa·s[28−33]. We only consider the temperature and pressure dependent viscosity in this study. Following Christensen[34], the dimensionless viscosity of the crust and upper mantle is estimated using the formula:

$$\eta = \frac{1}{\eta_0}\cdot\exp\left[\frac{E+W\cdot(1-z)}{2.088+T}\right], \qquad (1)$$

where η_0 is the reference viscosity, E and W denote the dimensionless activation energy and activation volume, respectively, z and T denote the dimensionless depth and temperature, respectively. Thus, in terms of eq. (1), the viscosity can be estimated from the temperature in the crust and upper mantle.

Figure 3 shows the temperature and viscosity distribution in our model, when η_0=10^{21} Pa·s, E=120, W=29.3. Here the viscosity of the crust beneath the mountain is assumed to be merely 10% of that beneath the basins on both sides.

3.3 Boundary condition and material partition

The top boundary in our model, as a free boundary, corresponds to the ground surface. The bottom boundary corresponds to the bottom of the upper mantle, it is assumed to be a free slip boundary. Both sides of our model are assumed also to be free slip boundaries. The temperature at the top and bottom is fixed in our model. The thermal fluxes on both sides are assumed to be zero.

We assume that the crustal thickness is 50 km and the crust is divided into three parts, including the mountain area and the basin area on both sides. In the upper mantle, the interfaces between different materials are consistent with the density contours shown in Figure 2. Totally, our model is composed of 11 materials.

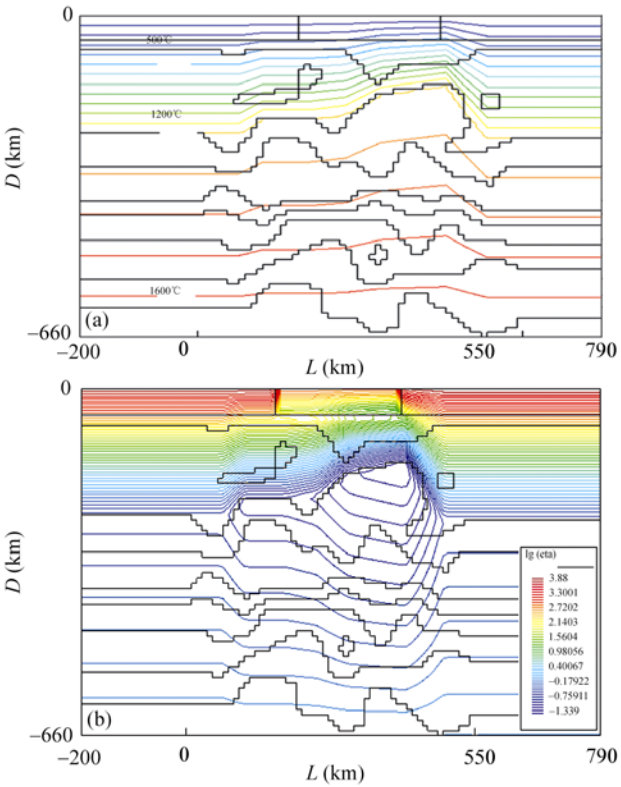

Figure 3 Temperature and viscosity distribution of the crust and upper mantle along Kuqa-Kuitun profile. Black solid lines indicate the bounds of different materials. (a) Temperature distribution (℃); (b) viscosity distribution (logarithmic value scaled by η_0).

4 Numerical modeling of the upper mantle convection

4.1 Analysis of convective patterns

Figure 4 shows the simulation results of the upper mantle convection driven by density anomalies. We can see a strong counterclockwise convection in the upper mantle underneath the Junggar basin and North Tianshan, whose scale reaches to ~500 km. Figure 4 also shows another relatively weak and small clockwise convection underneath the Tarim block. These two convection cells are joined together underneath the southern border of the Tianshan Mountains. This implies that under the drag effect of the mantle convection, the lithosphere beneath the Tarim and Junggar blocks thrusts down to the Tianshan Mountains. Due to the difference of the intensities between two convection cells, the subduction is asymmetric. The subduction of the Tarim lithosphere is ter-

minated at the southern border of the Tianshan Mountains. This observation is consistent with the supposition made according to the receiver function inversion[35] and the seismic tomography[18].

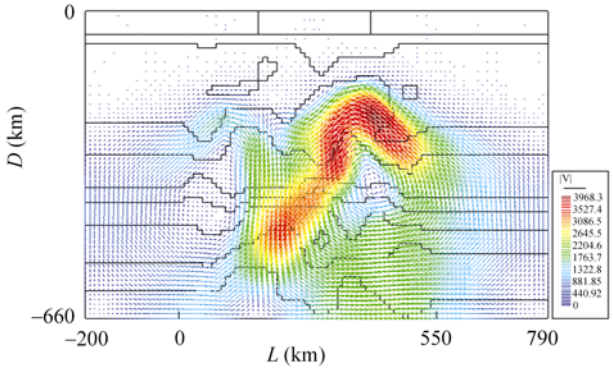

Figure 4 The upper mantle convection driven by density anomalies. Colorful legend denotes the value of dimensionless velocity. Dimensionless velocity multiplied by 0.0478 equals the velocity value with unit mm/a in this paper. Black lines indicate the bounds of different materials.

The velocity distribution nearby the ground surface shown in Figure 4 manifests that owing to the drag effect of the upper mantle convection, the Tarim and Junggar blocks have an opposite horizontal movement toward the Tianshan Mountains. The velocity difference between both sides of the mountain area, i.e. the shortening rate is less than 1 mm/a in the range of the mountains. The vertical descending deformation of the ground surface appears in the mountain area. It corresponds to the downwelling of the upper mantle beneath the Tianshan Mountains.

From the GPS data, Wang et al. [22] proposed that the Tarim basin moves northward and the Tianshan crust has a shortening rate of 4—20 mm/a. Their results manifest that the shortening rate of the Tianshan crust becomes smaller from west to east and it is 7—8 mm/a in the Kuqa-Kuitun profile. In addition, the present-day uplift of the Tianshan Mountains has also been verified by the results from the surface geology and level survey[9,36]. Therefore, the deformation of the ground surface shown in Figure 4 is contradictory with the practical deformation observations. This implies that the small-scale convection of the upper mantle underneath the Tianshan Mountains does not lead to its uplift, which must be caused by other dynamic source.

In fact, the proofs given by the geological studies have demonstrated that the thrust of the Tarim block plays the key role in the Tianshan uplift[6−9]. Therefore, we reset such a new boundary condition in our model that makes the Tarim crust move northward at the velocity of 7.17 mm/a. The computational result is shown in Figure 5.

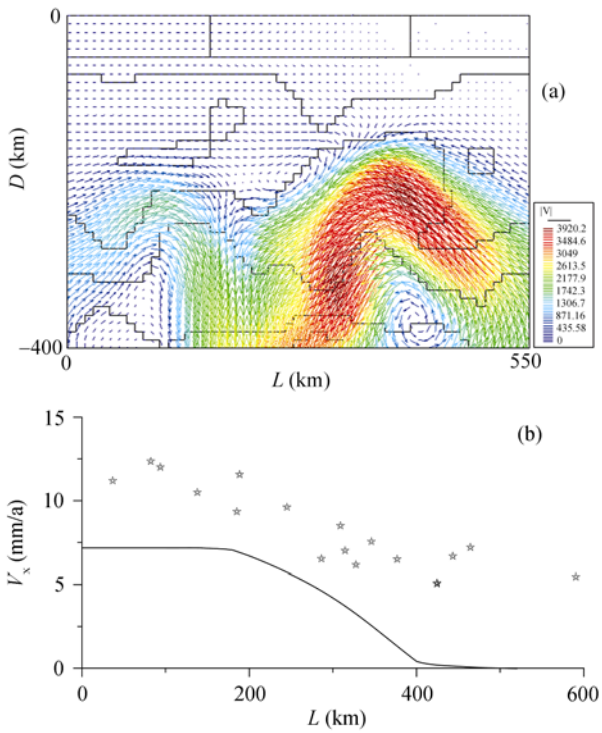

Figure 5 The upper mantle convection and velocity distribution on the top boundary considering the compression of the Tarim block (annotations are the same as in Figure 4). (a) The crust and upper mantle convection; (b) horizontal velocity distribution on the surface and GPS data (denoted by stars).

In comparison of Figure 5(a) with Figure 4, we can see that the convection cells in the same range in both figures have almost no difference, except that the northward movement of the Tarim lithosphere in Figure 5(a) is slightly faster than that shown in Figure 4. This manifests that the northward movement of the Tarim crust nearly does not influence the upper mantle convection. It can be inferred that the upper mantle convection will not be changed significantly, unless the strength and location of the applied thrust is close to the convection cell.

On the other hand, Figure 5(a) shows that the upper mantle convection significantly influences the northward movement of the Tarim block. Since the movement of the material beneath the Junggar lithosphere has a large southward velocity, it is able to resist effectively the northward movement of the Tarim block under the drag effect of the upper mantle. In this case, the Tarim litho-

sphere is arrested and drag downward by the downwelling of the mantle convection. Meanwhile, the far-field effect caused by the Tibetan uplift is eliminated by the shortening deformation of the Tianshan crust.

Figure 5(b) shows the computational horizontal velocity distribution and the GPS observations in the region of 82.2—85.5°E and 40.2—45.6°N, which are the projection on the Kuqa-Kuiton profile. Our computational result is consistent with the GPS observation in the tendency of the velocity variation and it manifests that the deformation of the Tianshan crust has absorbed the energy of the 'far-distance effect' through the Tarim block.

Our computational result of the vertical velocity distribution manifests that the Tianshan crust is in the uplift status. The uplift speed is increased gradually from south to north and its maximal value reaches to 1.13 mm/a.

In comparison of Figure 4 with Figure 5, we can see that the northward extrusion of the Tarim block plays a key role in the Cenozoic Tianshan mountain building.

Corresponding to Figure 5(a), Figure 6 shows the computational principal strain rate in the mountain area in the depth range over 0—120 km. Figure 6 manifests that both of the vertical and horizontal crustal deformation in the North Tianshan are larger than those in the South Tianshan. These could be related closely to the thinning lithosphere underneath the mountain area and the large convective velocity of the upper mantle. The result shown in Figure 6 indicates why the North Tianshan has an uplifting rate larger than the South Tianshan[36]. In addition, Figure 6 also manifests that the small-scale convection of the upper mantle beneath the Tianshan Mountains not only resists the northward movement of the Tarim block, but also distorts the crustal deformation by heating and thinning the lithosphere.

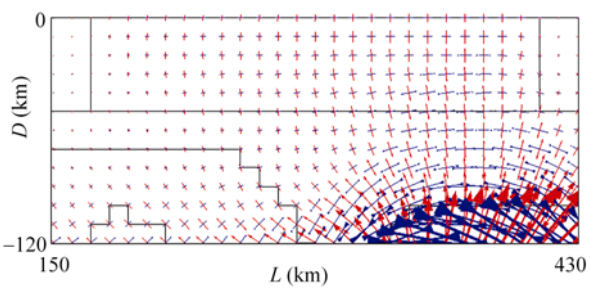

Figure 6 Principal strain rate of the crust and topmost of upper mantle of the Tianshan range. Blue arrows denote compressional principal strain rate, red arrows denote tensile's. The length of arrows is directly proportional to the value of the principal strain rate.

4.2 The speed and evolution of the convection

As shown in Figure 4 and Figure 5(a), the maximal speed of the convection in our model reaches to ~190 mm/a at the border of the northern Tianshan and Junggar block. Since the nonlinear viscosity model was not considered, the speed of mantle flow is inversely proportional with the viscosity.

In addition, Figure 3(b) is merely one of the possible viscosity distributions in the upper mantle underneath the Tianshan Mountains. Our numerical tests on the other possible models have demonstrated that the convective pattern is almost unchanged, although the upper mantle convection can have different speeds. Since it would be impossible that the viscosity of the upper mantle in the mountain range is larger than 3×10^{21} Pa·s averaged over the whole mantle[31], the maximal speed at the top of the upper mantle underneath the Tianshan Mountains is 20 mm/a corresponding to this viscosity, it can be inferred from this that the lower limitation of the convection speed of the upper mantle beneath the Tianshan Mountains is not less than 20 mm/a.

It should be pointed out that all of the results shown in Figures 4—6 are merely the computational output at the first time step for the transient state problem, which corresponds to the results obtained from contemporary geophysical data. At the subsequent time steps, the density contours will gradually become flattening and the mantle convection becomes weak.

5 Conclusion and discussion

Based on the result given by the P-wave travel time tomography of the upper mantle velocity structure along the Kuqa-Kuitun profile, the small-scale convection of the upper mantle underneath the Tianshan Mountains driven by the density anomalies is simulated using the FEM combining with MIC technique. Our results manifest that (1) there is a counterclockwise convection prompted by the present-day density anomalies in the upper mantle underneath the Junggar basin and North Tianshan, whose scale reaches to ~500 km; (2) underneath the Tarim basin and South Tianshan exists a clockwise northward convection, which is relatively weak; (3) the convective speed at the top of the upper mantle underneath the Tianshan Mountains should not be less than 20 mm/a, although the convective speed depends, to a great degree, on the viscosity of the upper mantle; (4) the northward extrusion of the Tarim block

plays a key role in the Cenozoic Tianshan mountain building and the present-day tectonic deformation of the Tianshan Mountains is closely related to the upper mantle convection; and (5) the northward subduction of the Tarim block nearly does not influence the upper mantle convection beneath the Tianshan Mountains.

Our main purpose in this study is to verify the small-scale upper mantle convection underneath the Tianshan Mountains in China in terms of the numerical simulation technique. Although we adopt a quantitative method, what we pursuit is not quantitative results, but a qualitative conclusion.

In addition, the complex geophysical and geological structures of the crust of Tianshan Mountains are simplified in our computation. Our numerical tests demonstrate that the crust and lithosphere do not take part in the mantle convection, when their viscosity is large enough.

As mentioned above, in principle, the mantle convection is a 3D problem. Obviously, it is impossible that the 3D modeling is replaced simply by a 2D modeling. However, the high-resolution study of the upper mantle structure is an essential observational basis for investigating the small-scale mantle convection. The problem of the 3D upper mantle convection beneath the Tianshan Mountains in China needs to be solved in the future.

We would like to thank Prof. David A. Yuen, Minnesota University, Prof. Deng Qidong with IGCEA, Prof. Shi Yaolin and Dr. Zhang Huai with Graduate University of Chinese Acadamy of Sciences for their valuable suggestions. We also thank Prof. Gan Weijun with IGCEA for their GPS data.

1 Liu Q Y. Dynamics problems of Tianshan intracontinental orogen. In: Zhang Z J, ed. Deep Earth Structure and Geodynamics Study of Chinese Mainland (in Chinese). Beijing: Science Press, 2004. 792－799
2 Molnar P, Tapponnier P. Cenozoic tectonics of Asia: effects of a continental collision. Science, 1975, 189: 419－425
3 Tapponnier P, Monlar P. Active faulting and Cenozonic tectonics of the Tien Shan, Mongolia, and Baykal regions. J Geophys Res, 1979, 84: 3425－3459
4 England P, Houseman G. Finite strain calculation of continental deformation, 2. Comparison with the India-Asia collision zone. J Geophys Res, 1986, 91(B3): 3664－3676
5 Guo L Z, Shi Y S, Lu H F, et al. Two kind of long distance tectonic effects of the collision between India and Tibet. In: Collection of Essays of Modern Geology (in Chinese). Nanjing: Nanjing University Press, 1992. 1－8
6 Avouac J P, Tapponnier P, Bai M, et al. Active thrusting and folding along the Northern Tien Shan and late Cenozoic rotation of the Tarim relative to Dzungarian and Kazakhstan. J Geophys Res, 1993, 98: 6755－6804
7 Hendrix M S, Dumitru T A, Graham S A. Late Oligocence-early Miocene unroofing in the Chinese Tianshan: An early effect of the India-Asia collision. Geology, 1994, 22: 487－490[DOI]
8 Yin A, Nie S, Craig P, et al. Late Cenozoic tectonic evolution of the southern Chinese Tianshan. Tectonics, 1998, 17(1): 1－27[DOI]
9 Deng Q D, Feng X Y, Zhang P Z, et al. Active Tectonics of the Chinese Tianshan Mountains (in Chinese with English abstract). Beijing: Seismological Press, 2000
10 Vinnik, L P, Saipekova A M. Structure of the lithosphere and asthenosphere of the Tien Shan. Annales Geophysicae, 1984, 2(6): 621－626
11 Roecker S W, Sabitova T M, Vinnik L P, et al. 3-Dimensional elastic wave velocity structure of the western and central Tianshan. J Geophys Res, 1993, 98(B9): 15779－15795
12 Kosarev G L, Petersen N V, et al. Receiver function for the Tien Shan analog broadband network: contrasts in the evolution of structures across the Talasso-Fergana fault. J Geophys Res, 1993, 98(B3): 4437－4448
13 Chen Y H, Roecker S W, Kosarev G L. Elevation of the 400km discontinuity beneath the central Tien Shan: Case of missing root. EOS, 1996, 77: 416
14 Fu R S, Huang J H, Xu Y M, et al. Study of the mantle dynamics in the region from Qinghai-Xizang Plateau to Tianshan Mountains. Chin J Geophys (in Chinese), 1998, 41:658－668
15 King S D, Ritsema J. African hot spot volcanism: Small-scale convection in the upper mantle beneath cratons. Science, 2000, 290: 1137－1140
16 Kerr R A. A lava lamp model for the deep earth. Science, 1999, 283: 1826－1827[DOI]
17 Li S C, Liu Q Y, Chen J H, et al. Passive Broadband Seismic Array Observation across Tianshan. Prog Geophysics (in Chinese with English abstract), 2005, 20:955－960
18 Guo B , Liu Q Y, Chen J H, et al. Seismic tomography of the crust and upper mantle structure underneath the Chinese Tianshan. Chin J Geophys (in Chinese), 2006, 49: 1693－1700
19 Liu J, Liu Q Y, Song H Z. Numerical method of modeling thermal creeping flow in heterogeneous medium. Chin J Geophys, 2006, 49: 913－921
20 Li Q, Liu R F, Du A L, et al. Seismic tomography of Xinjiang and adjacent region. Chinese J Geophys (in Chinese with English Abstract), 1994, 37: 311－320
21 Xu Y, Liu F T, Liu J H, et al. Seismic tomography beneath the orogenic belts and adjacent basins of northwestern China. Sci China Ser D-Earth Sci, 2001, 44(5): 468－480
22 Wang Q, Ding G Y, Qiao X J, et al. Recent rapid shortening of crust across the Tianshan Mountains and relative motion of tectonic blocks in the north and south. Chin Sci Bull, 2000, 45: 1995－1999
23 Birch F. The velocity of compressional waves in rocks to 10 kilobars, 1. J Geophys Res, 1960, 65: 1083－1102
24 Birch F. The velocity of compressional waves in rocks to 10 kilobars,

2. J Geophys Res, 1961, 66: 2199－2224
25 Schubert G, Turcott D L, Olsen P. Mantle Convection in the Earth and Planets. Oxford: Cambridge Univ. Press, 2001
26 Kumar P, Yuan X, Kind R, et al. The lithosphere-asthenosphere boundary in the Tien Shan-Karakoram region from S receiver functions: Evidence for continental subduction, Geophys Res Lett, 2005, 32, L07305, doi:10.1029/2004GL022291, 1－4
27 Jeanloz R, Morris S. Temperature distribution in the crust and mantle. Ann Rev Earth Plannet Sci, 1986, 14: 377－415[DOI]
28 King S D. Models of mantle viscosity. In: Ahrens T J eds. Mineral and Crystallography: A Handbook of Physical Constants. Washington: AGU, 1995. 227—235
29 Haskell N A. The motion of a viscous fluid under a surface load, I. Physics, 1935, 6: 265－269
30 Haskell N A. The motion of a viscous fluid under a surface load, II. Physics, 1936, 7: 56－61
31 Karato S. The Dynamic Structure of the Deep earth: An Interdisciplinary Approach. Princeton: Princeton University Press, 2003
32 Forte A M, Mitrovica J X. Deep-mantle high-viscosity flow and thermochemical structure inferred from seismic and geodynamic data. Nature, 2001, 410: 1049－1055[DOI]
33 Mitrovica J X, Forte A M. A new inference of mantle viscosity based upon joint inversion of convection and glacial isostatic adjustment data. Earth Plannet Sci Lett, 2004, 225: 177－189
34 Christensen U. Convection with pressure- and temperature- dependent non-Newtonian rheology. Geophys J R astr Soc, 1984, 77: 343－384
35 Li Y , Liu Q Y, Chen J H, et al. Shear wave velocity structure of the crust and upper mantle underneath the Tianshan orogenic belt. Sci China Ser D-Earth Sci, 2007, 50(3): 321－330
36 Peng S S. On the neotectonic movement in Tianshan that reflected by the geodesic deformation survey. Intracontinental Earthquake (in Chinese with English abstract), 1993, 7: 136－141